Optical Clearing Agent Perfusion Enhancement via Combination of Microneedle Poration, Heating and Pneumatic Pressure

Yasaman Damestani, BS,[1] Bissrat Melakeberhan, BS,[2] Masaru P. Rao, PhD,[1,3,4] and Guillermo Aguilar, PhD[1,3]
[1]*Department of Bioengineering, University of California—Riverside, Riverside, California 92521*
[2]*Biology Department, University of California—Riverside, Riverside, California 92521*
[3]*Department of Mechanical Engineering, University of California—Riverside, Riverside, California 92521*
[4]*Materials Science and Engineering Program, University of California—Riverside, Riverside, California 92521*

Background and Objective: Optical clearing agents (OCAs) have shown promise for increasing the penetration depth of biomedical lasers by temporarily decreasing optical scattering within the skin. However, their translation to the clinic has been constrained by lack of practical means for effectively perfusing OCA within target tissues *in vivo*. The objective of this study was to address this limitation through combination of a variety of techniques to enhance OCA perfusion, including heating of OCA, microneedling and/or application of pneumatic pressure over the skin surface being treated (vacuum and/or positive pressure). While some of these techniques have been explored by others independently, the current study represents the first to explore their use together.
Study Design/Materials and Methods: Propylene glycol (PG) OCA, either at room-temperature or heated to 45°C, was topically applied to hydrated, body temperature *ex vivo* porcine skin, in conjunction with various combinations of microneedling pre-treatment (0.2 mm length microneedles, performed prior to OCA application), vacuum pre-treatment (17–50 kPa, performed prior to OCA application), and positive pressure post-treatment (35–172 kPa, performed after OCA application). The effectiveness of OCA perfusion was characterized via measurements of transmittance, reduced scattering coefficient, and penetration depth at a number of medically-relevant laser wavelengths across the visible spectrum.
Results: Topical application of room-temperature (RT) PG led to an increase in transmittance across the visible spectrum of up to 21% relative to untreated skin. However, only modest increases were observed with addition of various combinations of microneedling pre-treatment, vacuum pre-treatment, and positive pressure post-treatment. Conversely, when heated PG was used in conjunction with these techniques, we observed significant increases in transmittance. Using an optimal PG perfusion enhancement protocol consisting of 45°C heated PG + microneedle pre-treatment + 35 kPa vacuum pre-treatment + 103 kPa positive pressure post-treatment, we observed up to 68% increase in transmittance relative to untreated skin, and up to 46% increase relative to topical RT PG application alone. Using the optimal PG perfusion enhancement protocol, we also observed up to 30% decrease in reduced scattering coefficient relative to untreated skin, and up to 20% decrease relative to topical RT PG alone. Finally, using the optimal protocol, we observed up to 25% increase in penetration depth relative to untreated skin, and up to 23% increase relative to topical RT PG alone.
Conclusions: The combination of heated PG, microneedling pre-treatment, vacuum pre-treatment, and positive pressure-post treatment were observed to significantly enhance the perfusion of topically applied PG. Although further studies are required to evaluate the efficacy of combined perfusion enhancement techniques *in vivo*, the current results suggest promise for facilitating the translation of OCAs to the clinic. Lasers Surg. Med. 46:488–498, 2014. © 2014 Wiley Periodicals, Inc.

Key words: optical clearing agents; perfusion enhancement; microneedles; pneumatic pressure

INTRODUCTION

Optical clearing agents (OCAs) are nonreactive hyperosmotic agents that are used to increase tissue transparency in a transient and reversible manner. Although the exact mechanisms are still not well understood, prevailing opinion suggests that clearing is achieved through reduced optical scattering arising from matching of OCA and tissue refractive indices (due to OCA ingress and water egress under osmotic pressure), and/or dehydration and ordering of tissue fibrils in the dermis [1–4]. By providing means for transiently clearing skin, OCAs have shown promise for

Conflict of Interest Disclosures: All authors have completed and submitted the ICMJE Form for Disclosure of Potential Conflicts of Interest and none were reported.
Contract grant sponsor: American Society for Lasers in Medicine and Surgery (ASLMS).
*Correspondence to Guillermo Aguilar, PhD, Department of Mechanical Engineering, University of California—Riverside, Riverside, CA. E-mail: gaguilar@engr.ucr.edu
Accepted 23 April 2014
Published online 27 May 2014 in Wiley Online Library (wileyonlinelibrary.com).
DOI 10.1002/lsm.22258

enhancing the performance of a variety of diagnostic techniques, such as optical coherence tomography [3,5], second harmonic generation microscopy [4,6], confocal microscopy [4,6] and two-photon excited fluorescence microscopy [7–10], as well as many other medical applications [2,5,11–18]. Optical clearing also represents a critical element of a new concept we have recently introduced, Windows to the Brain. In this concept, OCAs would allow transient clearing of the scalp overlying a transparent cranial implant, thus providing a minimally-invasive means for optically accessing the brain, on-demand, over large areas, and on a chronically-recurring basis, without need for repeated craniectomies [19].

However, despite this promise, the continuing lack of sufficiently effective and/or practical OCA perfusion techniques *in vivo* represents a limitation with regard to clinical translation. The high viscosity of OCAs results in poor penetration through the stratum corneum when applied topically, as well as slow perfusion within the epidermis. In *ex vivo* studies, rapid and effective clearing has only been achieved through complete immersion of excised tissue samples in OCA, which is not feasible for use *in vivo* [7–10]. Single dose subdermal injection has been shown to produce fast clearing *in vivo*; however, this has been accompanied by necrosis and scarring, thus limiting the utility of this technique [20]. Sonophoresis and application of 1500 μm microneedles have shown potential for increasing clearing relative to topical application of OCA alone; however, visible damage to the stratum corneum was observed [21]. Finally, removal of the stratum corneum via sandpaper abrasion has been shown to enhance the transdermal delivery of OCA [22]; however, inflammation was also observed.

Herein, we report the first systematic and quantitative study of OCA perfusion enhancement using various combinations of OCA heating, microneedling pre-treatment (i.e., prior to OCA application), vacuum pre-treatment (i.e., prior to OCA application), and/or positive pressure post-treatment (i.e., after OCA application). The motivation for OCA heating was based on recent studies demonstrating enhanced clearing performance with heating of glycerol up to 40–45°C [23]. Moritz and Henriques [24] have previously studied time-surface thresholds for thermal injury of human skin and demonstrated that 2 hours of exposure to 45°C at the surface of human skin has caused hyperemia without loss of epidermis. For this study, the exposure time of 45°C OCA to skin was limited to 30 minutes. As such, epidermal loss is not expected, although hyperemia could still occur *in vivo*. The rationale for microneedling was based on the presumption that this would produce shallow pores that enable circumvention of the stratum corneum in a minimally invasive manner. The rationale for vacuum pre-treatment was based on the presumption that the resulting tissue stretching could enlarge pores produced by prior microneedling and therefore increase the OCA perfusion [25,26]. Finally, the rationale for positive pressure post-treatment was based on the presumption that this could increase OCA flux through pores produced by prior microneedling.

MATERIALS AND METHODS

Skin Preparation

Ex vivo abdominal porcine skin with intact stratum corneum was used for all studies, due to its anatomical similarity to human skin [27]. Fresh skin was obtained from a local research facility (University of California Irvine, Department of Surgery). Upon receipt, the tissue was sealed to prevent dehydration and stored at 4°C. All tissues were used within 2 weeks of receipt. Prior to each experiment, the skin samples were thawed and the subcutaneous fat layer was removed to yield samples of $1.5\,\text{mm} \pm 0.1\,\text{mm}$ thickness, which included stratum corneum ($26.4 \pm 0.4\,\mu\text{m}$ thickness [28]), epidermis ($65.8 \pm 1.8\,\mu\text{m}$ thickness [28]), and dermis (balance of sample thickness). The prepared samples were then re-hydrated by immersion in room temperature (RT) saline for 30 minutes. For all experiments, RT was maintained at 18°C and relative humidity at 30%.

OCA Perfusion

While a number of hyperosmotic agents have shown potential for use as OCAs, Propylene glycol (PG) (Sigma–Aldrich) was selected for the current studies, due to its superior permeability [29,30]. In all experiments, 100 μl of PG was applied topically over an area of approximately $100\,\text{mm}^2$, and total PG exposure time was maintained at 30 minutes. Thirty minutes was chosen on the basis of decreasing clearing rate as well as maintaining the experiment parameters within the context of eventual clinical practicality. For studies involving RT OCA, PG was dispensed from a container held under ambient conditions (18°C). For studies involving heated OCA, PG was warmed to 45°C using a hot plate prior to topical application. This temperature was selected to minimize PG viscosity ($16.4\,\text{mPa}\cdot\text{s}$ at 44°C vs. $46.4\,\text{mPa}\cdot\text{s}$ at 24°C [31]) without surpassing the threshold for thermal damage to the skin.

For studies involving microneedling pre-treatment (i.e., prior to OCA application), a commercial microneedle roller was manually applied to the skin samples in 0°, 45°, and 90° rolling directions over the same area, with thirty roller passes applied in each direction (CR2 MTS roller, Clinical Resolution Laboratory, Brea, CA; ISO 13485:2003 approved, microneedle length = 0.2 mm, diameter = 0.07 mm, and pitch = 2.5 mm). The pore density produced by microneedling (Fig. 1a) were measured via topical dye application (trypan blue), followed by removal of excess dye, and finally, imaging with a Dermatoscope (3.5V Pro-Physician Dermatolight-LED Dermatoscope) coupled with a digital camera (Kodak MAX Z990). Untreated (i.e., non-microneedled) tissue specimens were processed in a similar manner to serve as control (Fig. 1b). The depth and diameter of pores produced by microneedling (Fig. 1c) was measured by topical application of Rhodamine R, followed by histological sectioning and imaging an average of twenty 40 μm thick slices per sample with a fluorescence microscope (Leica MZIII Pursuit). In each tissue section, an average of six pores was measured in randomized locations across the section, and measurements were only

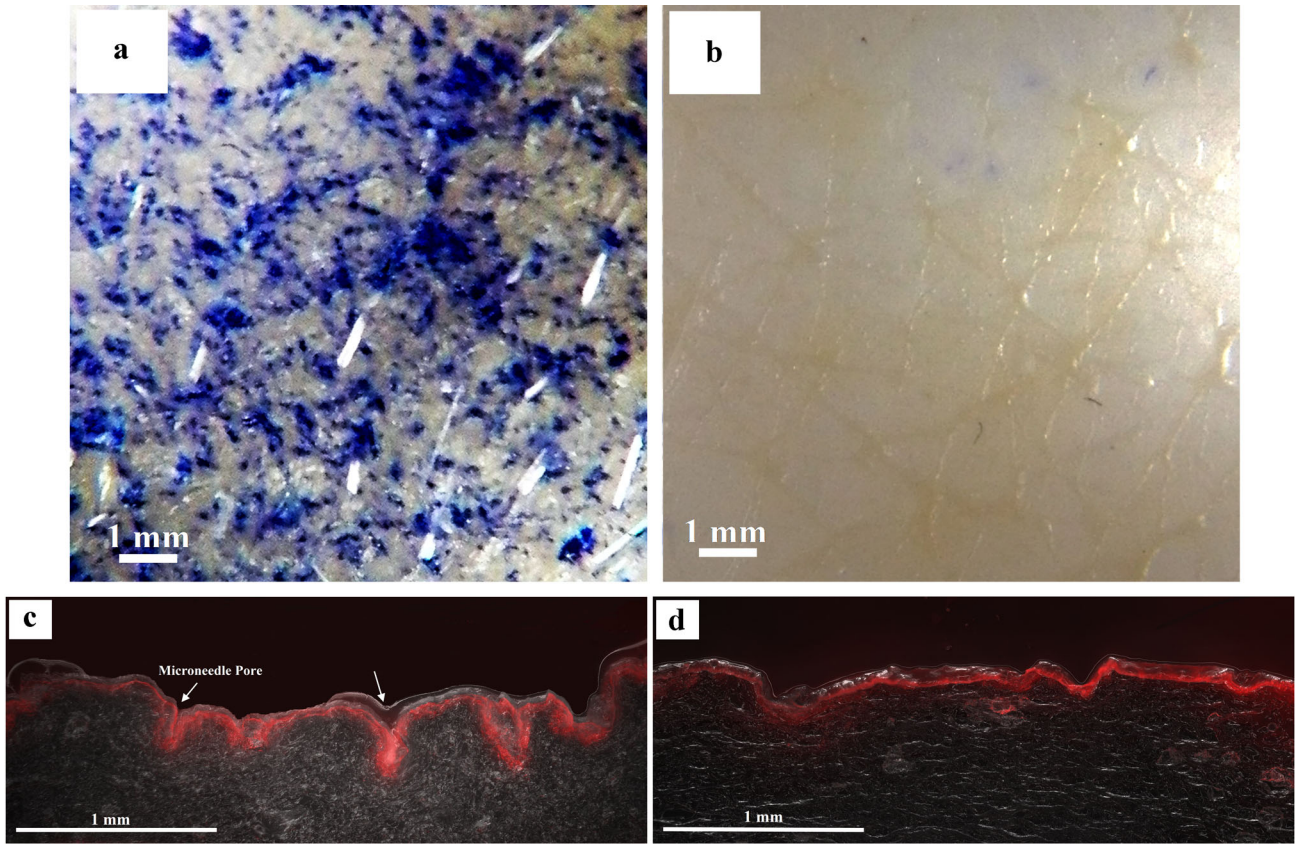

Fig. 1. Characterization of ex vivo porcine skin treated with 200 μm microneedle roller. **a**: Digital photograph of microneedled skin demonstrating average pore density of 240 ± 10 pores/cm^2. **b**: Digital photograph of untreated control skin. **c**: Histological cross section of microneedled skin demonstrating higher optical intensity due to higher perfusion of Rhodamine R compared to untreated tissue (**d**) and average pore diameters of 0.22 ± 0.08 mm on the surface of skin, and average pore depth of 0.20 ± 0.04 mm. **d**: Histological cross section of non-microneedled skin demonstrating native topographical variation.

taken for pores with clearly defined boundaries (i.e., sharp demarcation between Rhodamine R (red) and the adjacent background (black)). Since many pores tapered with depth into the skin, the reported pore diameters are those measured at the skin surface. Collectively, these measurements indicated average pore density of 240 ± 10 pores/cm^2, average pore diameter of 0.22 ± 0.08 mm on the surface of skin, and average pore depth of 0.20 ± 0.04 mm for microneedled skin. Histological imaging of non-microneedled skin samples was also performed to characterize the native topographical variation of the skin (Fig. 1d).

For studies involving pneumatic pressure, a custom apparatus (Fig. 2a) was fabricated from transparent acrylic to allow application of pressure (negative or positive) to the epidermal surface of the skin samples. During these studies, sample hydration was maintained from the dermal surface via contact with an underlying body-temperature, saline-saturated, rigid foam block (Oasis Wet Floral Foam, Smithers-Oasis North America, Kent, OH). For studies involving vacuum pre-treatment (i.e., prior to OCA application), vacuum ranging from 17 kPa to 50 kPa was applied for 1 minute using a hand pump (9963K21, McMaster-Carr, Los Angeles, CA). For studies involving positive pressure post-treatment (i.e., after OCA application), pressure ranging from 35 to 172 kPa was applied for 4 minutes using house compressed air with a regulator (Harris Gas Regulator, Harris Products Group, Gainesville, GA).

Optical Clearing Characterization

After application of prescribed perfusion enhancement protocols, residual PG was removed from the skin surface by gentle wiping with an absorbent cloth, and the samples were immediately transferred to an optical measurement system. Transmittance and reflectance spectra across wavelengths ranging from 450 to 850 nm were measured using a fiber optic spectrometer (SD2000, Ocean Optics, Dunedin, FL). A fiber optic bundle with a 150 W quartz halogen illuminator was used as the light source for transmission measurements (Model 180, Fiber-Lite, Dolan Jenner, Boxborough, MA). Reflection was measured with a Spectralon coated integrating sphere with a built-in tungsten-halogen light source for 400–800 nm wavelengths (ISP-REF Integrating Sphere, Ocean Optics).

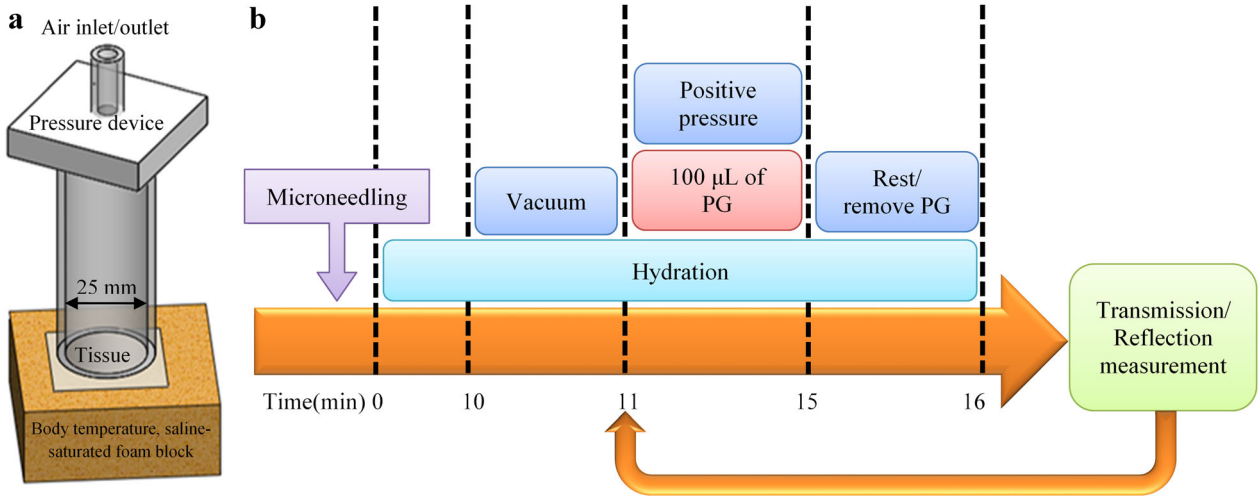

Fig. 2. **a**: Schematic of apparatus used for pneumatic pressure OCA perfusion enhancement studies in *ex vivo* porcine skin. Tissue samples were placed within the apparatus such that their dermal surface was in contact with the underlying body-temperature, saline-saturated foam block, while the epidermal surface was exposed to vacuum and/or positive pressure. **b**: Block diagram illustrating the sequence of operations for application of the various PG perfusion enhancement techniques. Briefly, the hydrated porcine skin was treated with microneedles and was kept hydrated from the dermis side using a body temperature, saline-saturated foam block for 10 minutes before the start of each experiment. For studies involving vacuum pre-treatment, vacuum was applied for 1 minute. For studies involving positive pressure post-treatment, pressure was applied for 4 minutes after the PG application. The tissue was rested for 1 minute, and PG was removed before the measurement of optical properties (transmission/reflection). The steps including the PG and positive pressure post-treatment application, rest and removal of PG, and the measurement of optical properties were repeated for 30 minutes (6 times).

The system was calibrated using a diffuse reflectance standard (WS-1, Ocean Optics). Measurements were made every 5 minutes for 30 minutes total, and all experiments were repeated in triplicate (Fig. 2b).

Wavelength Selection

Specific attention was focused on optical response at the following wavelengths due to their relevance for various laser-based medical imaging and therapeutic modalities: (1) 532 nm for laser-induced photoacoustic brain imaging [32]; (2) 630 nm for photosensitizer activation in photodynamic therapy of brain tumors [33]; (3) 650 nm for near-infrared spectroscopy and topographical imaging of brain [34]; (4) 670 nm for emerging photochemical internalization (PCI)-enhanced nonviral gene-directed enzyme prodrug cancer therapy [35]; and (5) 810 nm for brain interstitial laser photocoagulation therapies [36].

Data Analysis

Normalized transmittance, NT, was calculated using,

$$\mathrm{NT} = \frac{\mathrm{T_t}}{\mathrm{T_0}} \tag{1}$$

where T_t was the transmittance of the skin sample measured at time t after completion of a prescribed OCA treatment protocol, and T_0 was the transmittance measured before application of the prescribed OCA treatment protocol (i.e., untreated skin baseline transmittance). The reduced scattering coefficient, μ'_s, which combines the transmittance, reflectance, and thickness of the sample, was calculated using Prahl's inverse adding-doubling algorithm.

$$\mu'_s = \mu_s(1-g)[\mathrm{cm}^{-1}] \tag{2}$$

In these calculations, the anisotropy factor was assumed to be 0.9 for skin in the visible and NIR spectral range, and μ_s represented the scattering coefficient [37]. Finally, the photon penetration depth, δ, was estimated using the following expression [38]:

$$\delta = \frac{1}{\sqrt{3\mu_a(\mu_a + \mu'_s)}} \tag{3}$$

where μ_a represented the absorption coefficient at the measured wavelength, which was also calculated using the Prahl's inverse adding-doubling algorithm.

Statistical Analysis

All data was statistically analyzed using two-way repeated-measures ANOVA and Bonferroni post-tests. Statistics were calculated using a commercially-available software package (Prism 5.0, GraphPad, San Diego, CA).

Changes were considered statistically significant when the *P*-value was less than 0.05.

Qualitative Demonstration of Optical Clearing Efficacy

To provide a qualitative demonstration of the efficacy of optical clearing in skin treated with the optimal PG perfusion enhancement protocol, we utilized a thermocavitation technique we reported previously [39,40]. Briefly, treated *ex vivo* porcine skin was placed on the outer face of a quartz cuvette containing saturated aqueous copper nitrate solution ($CuNO_4$). The skin was then irradiated with an 810 nm CW laser operating at 12 W. Laser transmission through the cleared skin caused thermocavitation-induced bubble formation in the $CuNO_4$ solution, which was captured using a high speed video camera recording at 10^5 frames per second (Phantom V7, Version 9.1). Control experiments consisting of untreated skin subjected to identical conditions were also performed.

RESULTS AND DISCUSSION

Variation of Transmittance With Time

Figure 3 shows the variation of *NT* with time after topical application on *ex vivo* skin samples with RT PG. The change in NT is significantly different after 20 minutes for some wavelengths and after 30 minutes for all wavelengths ($P < 0.05$). The statistical analysis indicates the effect of time was extremely significant ($P < 0.001$) and the effect of wavelength was very significant ($P < 0.01$), with more pronounced improvement at shorter wavelengths. Maximum NT was observed at 30 minutes for most wavelengths, with up to 21% improvement relative to untreated skin ($P < 0.05$). Based on this preliminary study, measurement time of 30 minutes after treatment was selected for subsequent perfusion enhancement studies. The relatively modest increase in NT confirms the strong barrier function of the stratum corneum, which precludes significant clearing with topical RT PG alone.

Figure 4 shows the variation of NT with time after treatment of microneedled skin with RT PG. The change in NT is significantly different after 30 minutes for all wavelengths ($P < 0.05$), thus supporting the appropriateness of this measurement time point for subsequent microneedling-based perfusion enhancement studies. Interestingly, only minimal enhancement of transmittance was observed relative to RT PG alone (i.e., Fig. 3). Moreover, the effect of microneedling seemed to be more pronounced for longer wavelengths, although the underlying cause is unclear. While other studies using the same region of skin (abdominal) as in this study have shown up to two-fold increase in NT with microneedling [41], this may be due to the longer needle length used in those studies (i.e., 500 μm microneedle roller vs. 200 μm for the current study). While both needle lengths are sufficient to circumvent the stratum corneum and access the epidermis, longer needles may produce deeper pores, which could facilitate OCA perfusion. However, longer needles may also increase pain sensation, thus producing a potential tradeoff between clearing efficacy and invasiveness when used *in vivo*.

Variation of Transmittance With Vacuum Pre-Treatment Pressure

Figure 5 shows the variation of *NT* with vacuum pretreatment pressures for microneedled skin treated with RT PG, all 30 minutes after treatment. The data showed no statistically significant variation in *NT* with vacuum pretreatment pressure ($P > 0.05$). This suggests that minimal pore enlargement was produced within this pressure range, or alternatively, that any pore enlargement that was achieved was insufficient in and of itself to enhance perfusion of RT PG. As such, 35 kPa vacuum pre-treatment pressure was arbitrarily selected for subsequent perfusion enhancement studies.

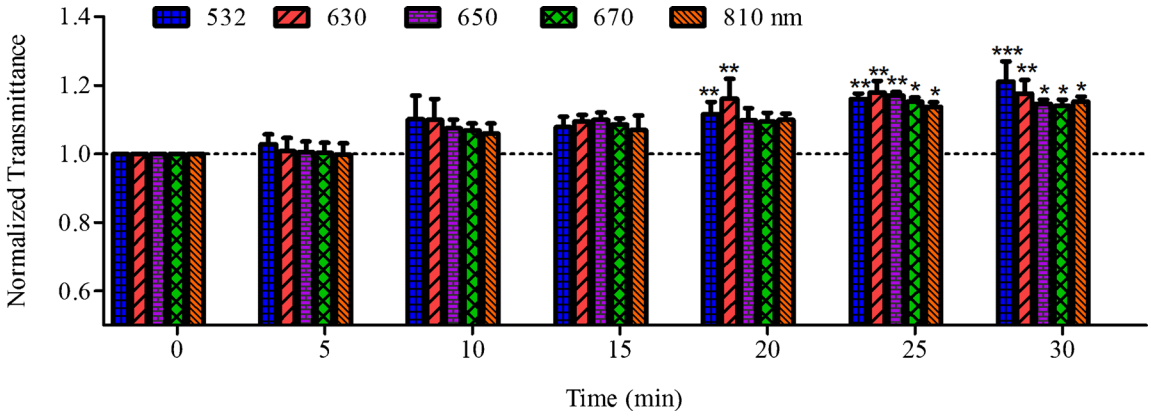

Fig. 3. Variation of NT at various medically relevant laser wavelengths with time after treatment of hydrated, ex vivo porcine skin with room temperature propylene glycol (PG). All data are normalized by transmittance for each skin sample before PG application (i.e., untreated skin). $N = 3$ for each condition and error bars represent 1 standard deviation, two-way ANOVA repeated measures, Bonferroni post-test $^{*}P < 0.05$, $^{**}P < 0.01$, $^{***}P < 0.001$ relative to 0 minute.

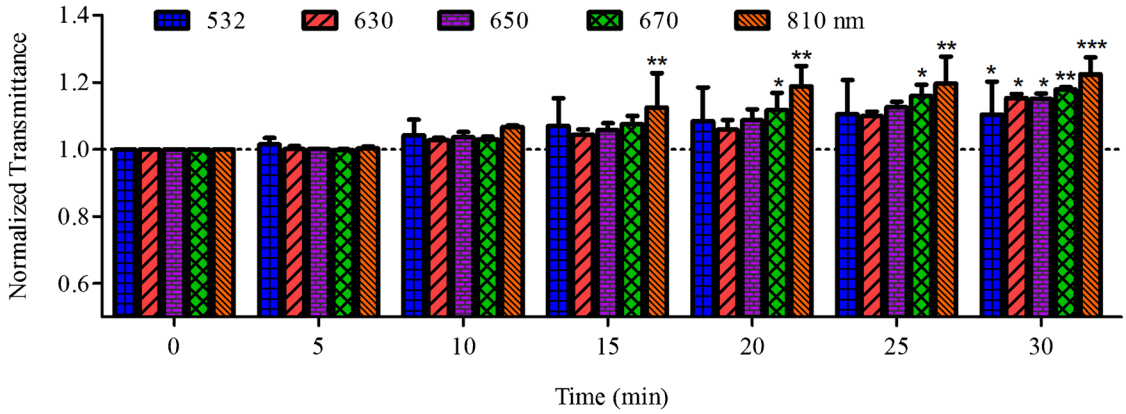

Fig. 4. Variation of NT with time after treatment of microneedled skin with room temperature PG. All data are normalized by transmittance for each skin sample before pre-treatment with microneedles (i.e., untreated skin). $N = 3$ for each condition and error bars represent 1 standard deviation. Two-way ANOVA repeated measures, Bonferroni post-test $^{*}P < 0.05$, $^{**}P < 0.01$, $^{***}P < 0.001$ relative to 0 minute.

Variation of Transmittance With Positive Pressure Post-Treatment

Figure 6 shows the variation of NT with positive post-treatment pressure for microneedled skin treated with RT PG, all 30 minutes after treatment. Maximum NT was observed at 103 kPa for most wavelengths, with up to 41% and 37% improvement relative to untreated skin and RT PG alone, respectively ($P < 0.01$). The decrease of *NT* beyond 103 kPa is likely due to observed PG splashing onto the sidewalls of the pneumatic apparatus at higher pressure, which may have reduced the amount available for perfusion. Based on this preliminary study, positive post-treatment pressure of 103 kPa was selected for subsequent perfusion enhancement studies.

According to federal Occupational Safety and Health Administration (OSHA), the air pressure threshold that can cause damage if directed at open wounds or body openings is 207 KPa (30 psi) and the pressure tolerances over muscles and bones in human subjects have been reported in the range of 0.5–1.1 MPa [42]. Since the pressures applied in the current study are below these thresholds, pain and damage are not expected *in vivo*, although further studies *in vivo* will be required for confirmation. In mechanical tissue optical clearing technique where compression is the only factor in enhancement of light transmission through biological tissue, pressure applied was reported to be 0.13 MPa [26]. However, it is important to note that optical measurements were performed while the skin was pressurized [27], whereas there was no applied pressure during measurement in the current study. While we presume that positive pressure facilitated tissue clearing by enhancing PG permeation, it

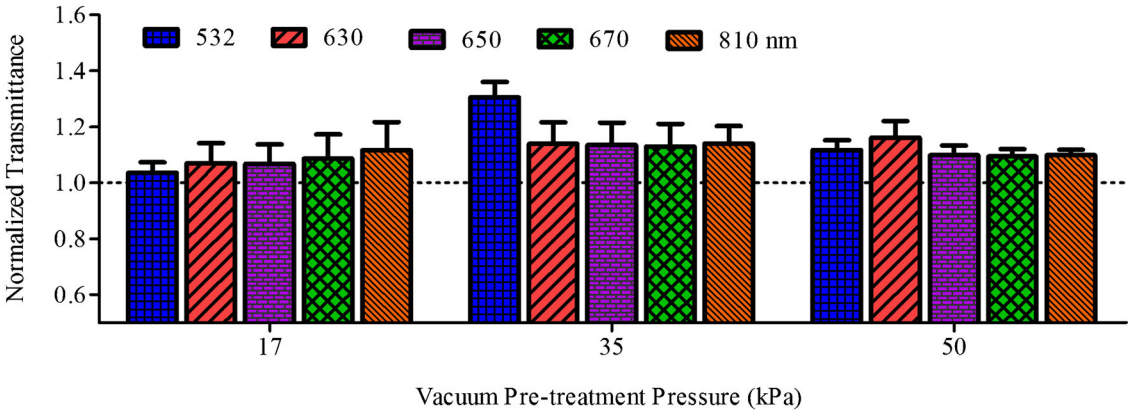

Fig. 5. Variation of transmittance with vacuum pre-treatment pressures for microneedled skin treated with room temperature PG. Measurements were made 30 minutes after treatment, and all data are normalized by transmittance for each skin sample before pre-treatment with vacuum and microneedles (i.e., untreated skin). $N = 3$ for each condition and error bars represent 1 standard deviation. Two-way ANOVA repeated measures, Bonferroni post-test $^{*}P < 0.05$, $^{**}P < 0.01$, $^{***}P < 0.001$ relative to 17 kPa. The NT results with different vacuum pre-treatment pressures for RT PG are not significantly different ($P > 0.05$).

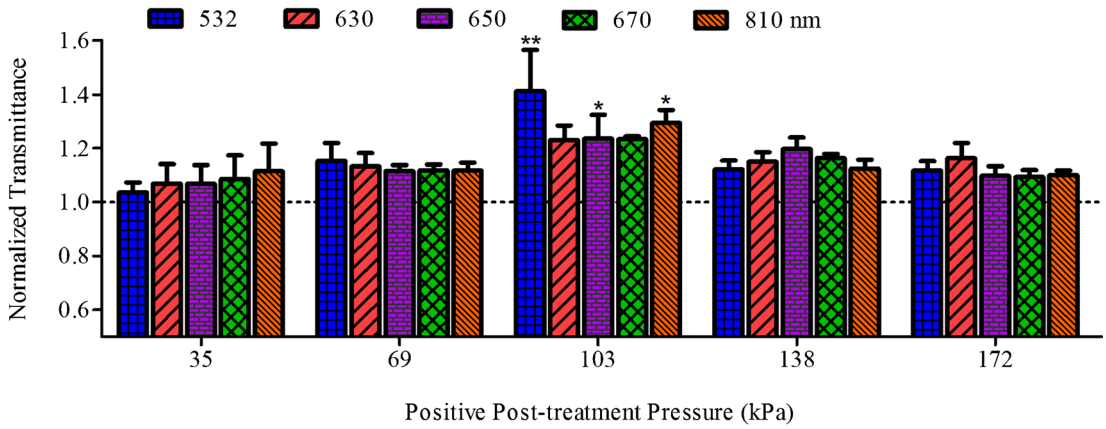

Fig. 6. Variation of transmittance with positive post-treatment pressures for microneedled skin treated with room temperature PG. Measurements were made 30 minutes after treatment, and all data are normalized by transmittance for each skin sample before pre-treatment with microneedles (i.e., untreated skin). $N = 3$ for each condition and error bars represent 1 standard deviation. Two-way ANOVA repeated measures, Bonferroni post-test $^{*}P < 0.05$, $^{**}P < 0.01$, $^{***}P < 0.001$ relative to 35 kPa.

is also conceivable that positive pressure enhanced PG solubility in collagen by increasing the PG interactions necessary for tissue clearing [40].

PG Perfusion Enhancement With Combination of Heating, Microneedling, and/or Pneumatic Pressure

Figure 7 summarizes the variation of NT due to each of the perfusion enhancement techniques individually, as well as in various combinations, all 30 minutes after treatment. Up to 21% increase in NT was observed across most wavelengths after application of RT PG, and there was only modest additional increase with use of 45°C heated PG (45°C). This suggests that reduced viscosity was insufficient in and of itself for enhancing PG diffusion through the stratum corneum ($P > 0.05$), as would be expected. The results also demonstrated that use of microneedling pre-treatment (MN), 35 kPa vacuum pre-treatment (VP), and/or 103 kPa positive pressure

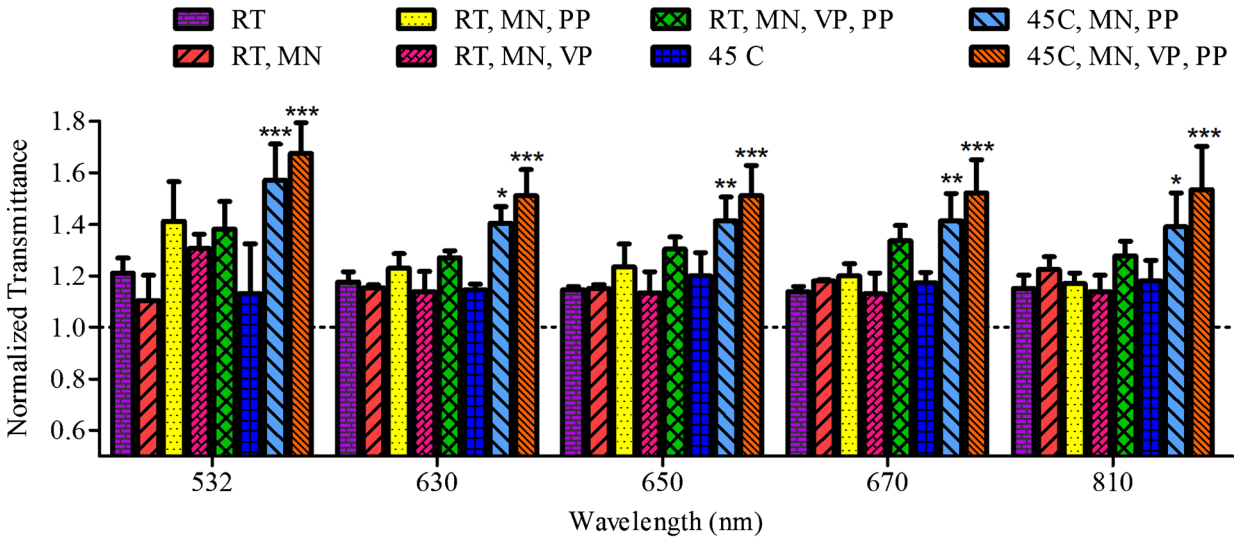

Fig. 7. Variation of transmittance for skin treated with room-temperature (RT) or 45°C heated PG (45°C), as well as with various perfusion enhancement techniques, including: pre-treatment with 0.2 mm microneedles (MN); pre-treatment with 35 kPa vacuum pressure (VP); and/or post-treatment with 103 kPa positive pressure (PP). Measurements were made 30 minutes after treatment, and all data are normalized by transmittance for each skin sample before PG application and/or any perfusion enhancement pre-treatment techniques (i.e., untreated skin). Maximum transmittance was observed with the optimal PG perfusion enhancement protocol shown in the right-most bar at each wavelength, which consisted of heated PG in combination with microneedle and vacuum pre-treatment, followed by positive pressure post-treatment. $N = 3$ for each condition and error bars represent 1 standard deviation. Two-way ANOVA repeated measures, Bonferroni post-test $^{*}P < 0.05$, $^{**}P < 0.01$, $^{***}P < 0.001$ relative to RT PG.

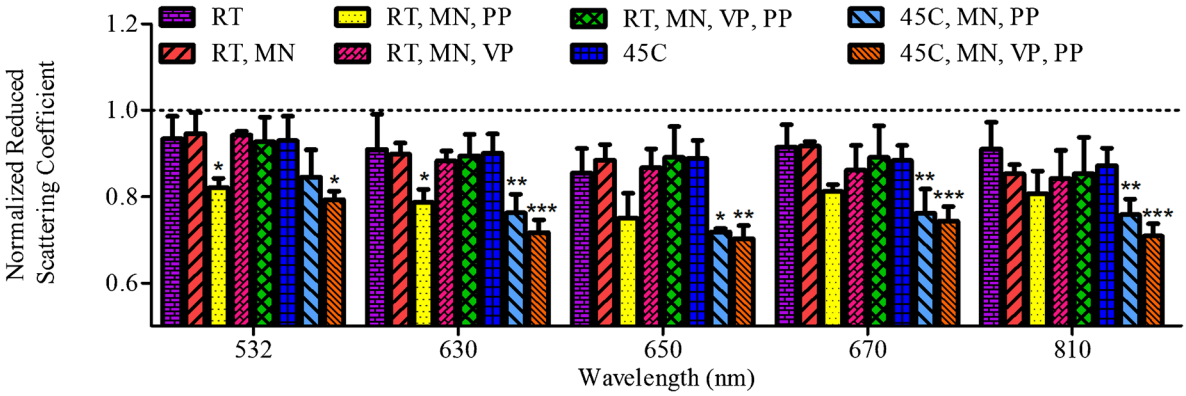

Fig. 8. Variation of calculated reduced scattering coefficient (μ'_s) for skin treated with room-temperature (RT) or 45°C heated PG (45°C), as well as with various perfusion enhancement techniques, including: pre-treatment with 0.2 mm microneedles (MN); pre-treatment with 35 kPa vacuum pressure (VP); and/or post-treatment with 103 kPa positive pressure (PP). Measurements were made 30 minutes after treatment, and all data are normalized by reduced scattering coefficient for each skin sample before PG application and/or any perfusion enhancement pre-treatment techniques (i.e., untreated skin). Minimum scattering was observed with the optimal PG perfusion enhancement protocol shown in the right-most bar at each wavelength. $N = 3$ for each condition and error bars represent 1 standard deviation. Two-way ANOVA repeated measures, Bonferroni post-test $^{*}P < 0.05$, $^{**}P < 0.01$, $^{***}P < 0.001$ relative to RT PG.

post-treatment (PP), either separately or combined, lead to only modest enhancement of perfusion of RT PG at most wavelengths ($P > 0.05$). However, the data show that significant increases in NT were achieved when these techniques were used in conjunction with heated PG. This suggests that reduced viscosity facilitated the effectiveness of the microneedling and pneumatic pressure perfusion enhancement techniques. Finally, for all wavelengths, maximum NT was achieved using an optimal PG perfusion enhancement protocol consisting of topical application of 45°C heated PG in conjunction with microneedle and 35 kPa vacuum pre-treatment, followed by 103 kPa positive pressure post-treatment ($P < 0.001$). Improvements in NT up to 68% relative to untreated skin, and up to 46% relative to topical application of RT PG, were observed.

Figures 8 and 9 show the variation in calculated μ'_s and δ, respectively, due to each of the perfusion enhancement techniques individually, as well as in various combinations, all 30 minutes after treatment. Similar to the trends observed for NT, μ'_s and δ were only moderately improved

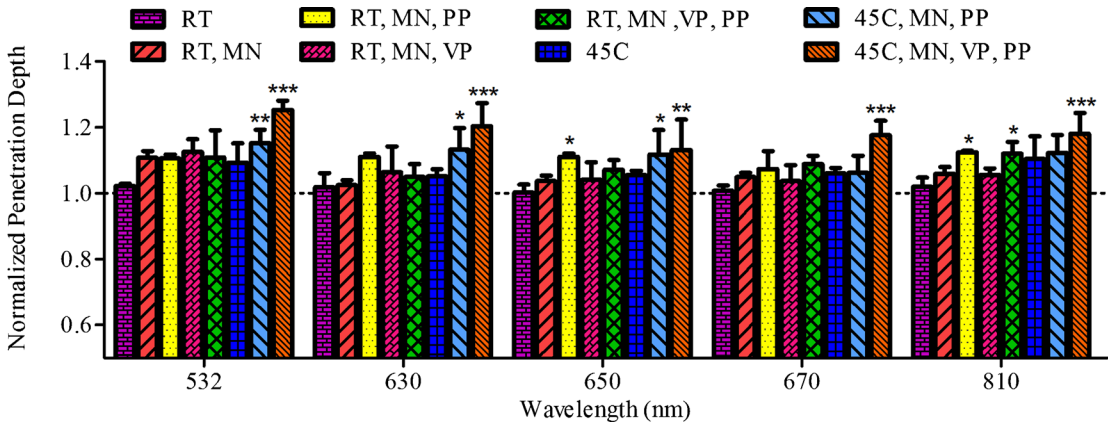

Fig. 9. Variation of calculated penetration depth (δ) for skin treated with room-temperature (RT) or 45°C heated PG (45°C), as well as with various perfusion enhancement techniques, including: pre-treatment with 0.2 mm microneedles (MN); pre-treatment with 35 kPa vacuum pressure (VP); and/or post-treatment with 103 kPa positive pressure (PP). Measurements were made 30 minutes after treatment, and all data are normalized by penetration depth for each skin sample before PG application and/or any perfusion enhancement pre-treatment techniques (i.e., untreated skin). Maximum penetration was observed with the optimal PG perfusion enhancement protocol shown in the right-most bar at each wavelength. $N = 3$ for each condition and error bars represent 1 standard deviation. Two-way ANOVA repeated measures, Bonferroni post-test $^{*}P < 0.05$, $^{**}P < 0.01$, $^{***}P < 0.001$ relative to RT PG.

with each perfusion enhancement technique individually. However, when used together, in conjunction with heating, up to 30% decrease in μ'_s was observed relative to untreated skin, and up to 20% decrease was observed relative to topical RT PG (at least $P < 0.05$ for all wavelengths). Similarly, up to 25% increase in δ was observed relative to untreated skin, and up to 23% increase was observed relative to topical RT PG (at least $P < 0.05$ for all wavelengths).

Collectively, Figures 7–9 demonstrate that significant improvement in clearing can be achieved using the optimal PG perfusion enhancement protocol. It is interesting to note that while the magnitude of clearing varies with laser wavelength, the correlation between wavelength and perfusion condition was not considered significant ($P = 0.8$). Nevertheless, the optimal perfusion condition (45°C, MN, VP, PP) has a definite enhancement trend across all wavelengths, albeit not in the same proportion.

Qualitative Demonstration of Optical Clearing Efficacy

Figure 10a shows a schematic illustration of the experimental set up used for demonstration of optical clearing efficacy via thermocavitation. Figure 10b shows a sequence of stills captured from high-speed video recording of thermocavitation-induced bubble formation in $CuNO_4$ solution produced during laser fluence through hydrated, *ex vivo* porcine skin treated with the optimal PG perfusion enhancement protocol. Bubble formation was observed soon after laser turn-on and ceased soon after the laser was turned off. In contrast, no bubble formation was observed when untreated skin was used, and significant thermal damage was observed (data not shown). This demonstrates that well-controlled perfusion of PG within skin can increase the photon density delivered to a specific subsurface target while minimizing or confining the thermal damage. Determining the effect of less efficient PG perfusion enhancement protocol is beyond the scope of the current study, since the thermocavitation experiments were simply intended to serve as a proof-of-concept level demonstration of the enhanced clearing, independent of a particular application.

The current study has provided preliminary evidence supporting the potential afforded by combined microneedling, OCA heating, and pneumatic pressure for enhancing optical clearing performance. However, it is important to emphasize that these studies fail to reproduce the full complexity of the *in vivo* environment, and as such, further study is required to determine whether these techniques will yield similar improvements in clinical settings. Of particular importance in this regard, will be the effect of active perfusion by the vasculature *in vivo*, which may facilitate OCA transport away from the delivery site, and thus, reduce clearing efficacy. Moreover, while no visible skin damage was observed and most of the techniques used in this study have been demonstrated by others to be minimally invasive on an individual basis, it is unclear whether their use together will be similarly innocuous. Also, future studies need to be performed to examine the effect of various temperature between RT and 45°C on the skin and the perfusion of PG. Lower PG is expected to reduce the clearing efficacy, due to increased viscosity of PG. Finally, it is unclear whether the magnitude and depth of clearing that could be achieved *in vivo* using such techniques will be sufficient for all

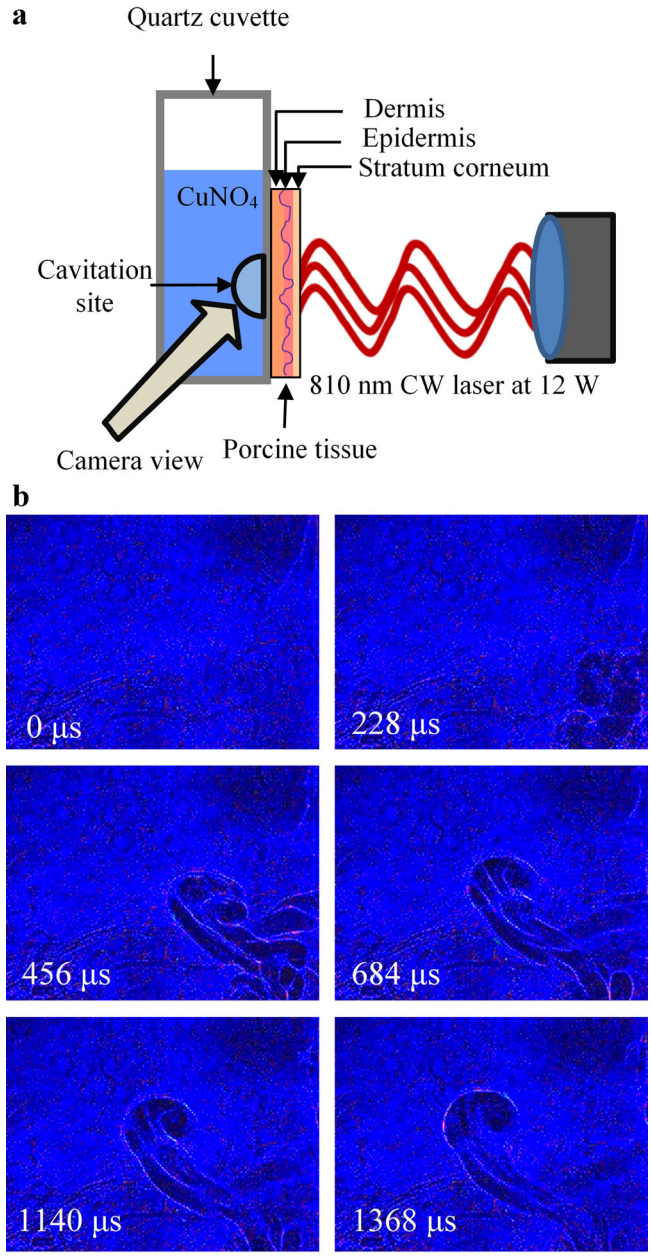

Fig. 10. Qualitative demonstration of optical clearing efficacy via thermocavitation. **a**: Schematic illustrating experimental set up. **b**: Sequence of stills captured from high-speed video recording of thermocavitation shockwave in aqueous copper nitrate ($CuNO_4$) solution produced during laser fluence through skin treated with optimal PG perfusion enhancement protocol. In similar experiments performed with untreated skin (not shown), bubble formation was not observed, and skin charring occurred.

applications. For example, it is conceivable that through-thickness clearing of thin tissues could be achieved using the current techniques (e.g., clearing of scalp for the aforementioned Windows to the Brain concept). However, for deeper clearing in thicker tissues, it is likely that longer microneedles would be required, which could increase pain and invasiveness.

CONCLUSIONS

In this study, we demonstrated, for the first time, the quantitative comparison of a variety of techniques to enhance optical clearing, including microneedling, OCA heating, and pneumatic pressure application. Application of the optimal combination of these techniques on *ex vivo* porcine tissue resulted in 68% increase in NT relative to untreated skin, and up to 46% increase relative to topical RT PG application alone. Enhancements in μ'_s and δ were also observed. Collectively, this suggests potential for enhancing optical clearing performance *in vivo*, and thus, potential for facilitating the use of medical lasers in numerous clinical applications.

ACKNOWLEDGMENTS

The authors would like to acknowledge the American Society for Laser Medicine and Surgery (ASLMS) for a travel grant awarded to Y. D. to present research leading to this study at the 33rd Annual ASLMS Conference, Boston, MA, April 2013. Additionally, the authors thank Mr. Earl Steward, Lab Director in the Department of Surgery, University of California Irvine, School of Medicine, for providing the porcine tissue. The authors also acknowledge Mr. Roberto Ayala for his contribution to data collection, Mr. Darren Banks for his contribution to thermocavitation studies, and Mr. Omid Khandan for his contribution to microneedle poration characterization.

REFERENCES

1. Chance B, Robertson C, Gopinath S, Liu H, Zhang Y, Mayevsky A. Optical response to osmotic stress and cortical depolarization in animal brain. Biophys J 1996;70:Wp154.
2. Tuchin VV, Maksimova IL, Zimnyakov DA, Kon IL, Mavlyutov AH, Mishin AA. Light propagation in tissues with controlled optical properties. J Biomed Opt 1997;2:401–417.
3. He Y, Wang RK. Dynamic optical clearing effect of tissue impregnated with hyperosmotic agents and studied with optical coherence tomography. J Biomed Opt 2004;9:200–206.
4. Meglinski IV, Bashkatov AN, Genina EA, Churmakov DY, Tuchin VV. The enhancement of confocal images of tissues at bulk optical immersion. Laser Phys 2003;13:65–69.
5. Vargas G, Chan EK, Barton JK, Rylander HG, III, Welch AJ. Use of an agent to reduce scattering in skin. Lasers Surg Med 1999;24:133–141.
6. Zuluaga AF, Drezek R, Collier T, Lotan R, Follen M, Richards-Kortum R. Contrast agents for confocal microscopy: How simple chemicals affect confocal images of normal and cancer cells in suspension. J Biomed Opt 2002;7:398–403.
7. Tuchin VV. Optical clearing of tissues and blood using the immersion method. J Phys D Appl Phys 2005;38:2497–2518.
8. Jiang J, Wang RK. Comparing the synergistic effects of oleic acid and dimethyl sulfoxide as vehicles for optical clearing of skin tissue in vitro. Phys Med Biol 2004;49:5283–5294.
9. Yeh AT, Choi B, Nelson JS, Tromberg BJ. Reversible dissociation of collagen in tissues. J Invest Dermatol 2003; 121:1332–1335.
10. Xu X, Zhu Q. Evaluation of skin optical clearing enhancement with Azone as a penetration enhancer. Opt Commun 2007; 279:223–228.
11. Maier JS, Walker SA, Fantini S, Franceschini MA, Gratton E. Possible correlation between blood glucose concentration and the reduced scattering coefficient of tissues in the near infrared. Opt Lett 1994;19:2062–2064.
12. Yaroslavsky IV, Yaroslavsky AN, Tuchin VV, Schwarzmaier HJ. Effect of the scattering delay on time-dependent photon migration in turbid media. Appl Opt 1997;36:6529–6538.
13. Zimnyakov DA, Tuchin VV, Mishin AA. Spatial speckle correlometry in applications to tissue structure monitoring. Appl Opt 1997;36:5594–5607.
14. Vargas G, Chan KF, Thomsen SL, Welch AJ. Use of osmotically active agents to alter optical properties of tissue: Effects on the detected fluorescence signal measured through skin. Lasers Surg Med 2001;29:213–220.
15. Wang RK, Wilson M. Vertex/propagator model for least-scattered photons traversing a turbid medium. J Opt Soc Am A Opt Image Sci Vis 2001;18:224–231.
16. Wang RK. Signal degradation by multiple scattering in optical coherence tomography of dense tissue: A Monte Carlo study towards optical clearing of biotissues. Phys Med Biol 2002;47:2281–2299.
17. Xu X, Wang RK, El Haj A. Investigation of changes in optical attenuation of bone and neuronal cells in organ culture or three-dimensional constructs in vitro with optical coherence tomography: Relevance to cytochrome oxidase monitoring. Eur Biophys J 2003;32:355–362.
18. Khan MH, Chess S, Choi B, Kelly KM, Nelson JS. Can topically applied optical clearing agents increase the epidermal damage threshold and enhance therapeutic efficacy? Lasers Surg Med 2004;35:93–95.
19. Damestani Y, Reynolds CL, Szu J, Hsu MS, Kodera Y, Binder DK, Park BH, Garay JE, Rao MP, Aguilar G. Transparent nanocrystalline yttria-stabilized-zirconia calvarium prosthesis. Nanomedicine 2013;9:1135–1138.
20. McNichols RJ, Fox MA, Gowda A, Tuya S, Bell B, Motamedi M. Temporary dermal scatter reduction: Quantitative assessment and implications for improved laser tattoo removal. Lasers Surg Med 2005;36:289–296.
21. Han T, Das DB. Permeability enhancement for transdermal delivery of large molecule using low-frequency sonophoresis combined with microneedles. J Pharm Sci 2013;102:3614–3622.
22. Stumpp O, Chen B, Welch AJ. Using sandpaper for noninvasive transepidermal optical skin clearing agent delivery. J Biomed Opt 2006;11:041118.
23. Deng Z, Liu C, Tao W, Zhu D. Improvement of skin optical clearing efficacy by topical treatment of glycerol at different temperatures. J Phys Conf Ser 2011;277:1–8.
24. Moritz AR, Henriques FC. Studies of thermal injury: II. The relative importance of time and surface temperature in the causation of cutaneous burns. Am J Pathol 1947;23:695–720.
25. Aguilar G, Choi B, Broekgaarden M, Yang O, Yang B, Ghasri P, Chen JK, Bezemer R, Nelson JS, van Drooge AM, Wolkerstorfer A, Kelly KM, Heger M. An overview of three promising mechanical, optical, and biochemical engineering approaches to improve selective photothermolysis of refractory port wine stains. Ann Biomed Eng 2012;40: 486–506.
26. Rylander CG, Milner TE, Baranov SA, Nelson JS. Mechanical tissue optical clearing devices: Enhancement of light penetration in ex vivo porcine skin and adipose tissue. Lasers Surg Med 2008;40:688–694.
27. Netzlaff F, Schaefer UF, Lehr CM, Meiers P, Stahl J, Kietzmann M, Niedorf F. Comparison of bovine udder skin with human and porcine skin in percutaneous permeation experiments. Altern Lab Anim 2006;34:499–513.
28. Bronaugh RL, Stewart RF, Congdon ER, Giles AL, Jr. Methods for in vitro percutaneous absorption studies. I. Comparison with in vivo results. Toxicol Appl Pharmacol 1982;62:474–480.

29. Guo X, Guo Z, Wei H, Yang H, He Y, Xie S, Wu G, Deng X, Zhao Q, Li L. In vivo comparison of the optical clearing efficacy of optical clearing agents in human skin by quantifying permeability using optical coherence tomography. Photochem Photobiol 2011;87:734–740.
30. Zhi ZW, Han ZZ, Luo QM, Zhu D. Improve optical clearing of skin in vitro with propylene glycol as a penetration enhancer. J Innov Opt Health Sci 2009;2:269–278.
31. Sun TF, Teja AS. Density, viscosity and thermal conductivity of aqueous solutions of propylene glycol, dipropylene glycol, and tripropylene glycol between 290 K and 460 K. J Chem Eng Data 2004;49:1311–1317.
32. Wang X, Pang Y, Ku G, Xie X, Stoica G, Wang LV. Noninvasive laser-induced photoacoustic tomography for structural and functional in vivo imaging of the brain. Nat Biotechnol 2003;21:803–806.
33. Schmidt MH, Bajic DM, Reichert KW, II, Martin TS, Meyer GA, Whelan HT. Light-emitting diodes as a light source for intraoperative photodynamic therapy. Neurosurgery 1996; 38:552–556, discussion 556–557.
34. Wolf M, Ferrari M, Quaresima V. Progress of near-infrared spectroscopy and topography for brain and muscle clinical applications. J Biomed Opt 12:062104. 2007.
35. Hirschberg H, Kwon YJ. Photochemical internalization (PCI)-enhanced nonviral gene-directed enzyme prodrug cancer therapy. Mol Ther 2013;21:S85–S86.
36. Wyman DR, Schatz SW, Maguire JA. Comparison of 810 nm and 1064 nm wavelengths for interstitial laser photocoagulation in rabbit brain. Lasers Surg Med 1997; 21:50–58.
37. Prahl SA, Vangemert MJC, Welch AJ. Determining the optical-properties of turbid media by using the adding-doubling method. Appl Optics 1993;32:559–568.
38. Welch AJ, van Gemert MJC. *Optical-thermal response of laser-irradiated tissue*, 2nd edition. Dordrecht Heidelberg London New York: Springer; 2011.
39. Padilla-Martinez JP, Ramirez-San-Juan JC, Korneev N, Banks D, Aguilar G, Ramos-Garcia R. Breaking the Rayleigh-Plateau instability limit using thermocavitation within a droplet. Atomization Spray 2013;23:487–503.
40. Devia-Cruz LF, Perez-Gutierrez FG, Garcia-Casillas D, Aguilar G, Camacho-Lopez S, Banks D. High resolution optical experimental technique for computing pulsed laser-induced cavitation bubble dynamics in a single shot. Atomization Spray 2013;23:475–485.
41. Yoon J, Son T, Choi EH, Choi B, Nelson JS, Jung B. Enhancement of optical skin clearing efficacy using a microneedle roller. J Biomed Opt 2008;13:021103.
42. Izquierdo-Roman A, Vogt WC, Hyacinth L, Rylander CG. Mechanical tissue optical clearing technique increases imaging resolution and contrast through ex vivo porcine skin. Lasers Surg Med 2011;43:814–823.